Handling Qualities Assessment of a Pilot Cueing System for Autorotation Maneuvers

Jonathan Rogers, Laura Strickland, Caroline Repola
Georgia Institute of Technology
Atlanta, Georgia, United States

Michael Jump, Neil Cameron, Thomas Fell
The University of Liverpool
Liverpool, United Kingdom

ABSTRACT

This paper details the design and limited flight testing of a preliminary system for visual pilot cueing during autorotation maneuvers. The cueing system is based on a fully-autonomous, multi-phase autorotation control law that has been shown to successfully achieve autonomous autorotation landing in unmanned helicopters. To transition this control law to manned systems, it is employed within a cockpit display to drive visual markers which indicate desired collective pitch and longitudinal cyclic positions throughout the entire maneuver, from autorotation entry to touchdown. A series of simulator flight experiments performed at University of Liverpool's HELIFLIGHT-R simulator are documented, in which pilots attempt autorotation with and without the pilot cueing system in both good and degraded visual environments. Performance of the pilot cueing system is evaluated based on both subjective pilot feedback and objective measurements of landing survivability metrics, demonstrating suitable preliminary performance of the system.

NOTATION

h	Altitude above ground level (-z) [ft]
q	Pitch rate in body reference frame [rad/s]
t_{gc}	Ground contact time [s]
V_{des}	Forward speed command [ft/s]
$\widehat{V}_{ss}$	Desired forward flight speed during steady state autorotation [ft/s]
$\widehat{V}_{td}$	Desired forward flight speed at touchdown [ft/s]
η_{max}	Maximum pitch angle commanded by the controller [deg]
Ω	Main rotor rotation rate [rad/s]
$\widehat{\Omega}_{des}$	Desired rotor speed [rad/s]
$\dot{\theta}_0$	Collective control derivative [rad/s]
θ_0	Main rotor collective blade pitch [deg]
θ_{1s}	Main rotor longitudinal cyclic pitch [deg]

INTRODUCTION

Autorotation is a complex flight maneuver that offers little margin for error. For many rotorcraft platforms, especially those with high disk loading, incorrect timing of the autorotation flare and deceleration maneuvers may result in significant aircraft damage and injury to the crew. The increasing use of multi-engine rotorcraft by the US military and improvements in reliability has reduced the frequency of autorotation emergencies. However, autorotation remains a complex and difficult maneuver in certain conditions such as degraded visual environments (DVE), nighttime operations, or low-energy flight conditions, all of which reduce the chances of a successful autorotation outcome. Despite improved training and procedures, the US military still suffers fatal autorotation accidents, even in multi-engine helicopters. For instance, the 2014 crash of an Idaho Air National Guard AH-64 that killed two veteran pilots occurred due to a suspected incorrectly-performed autorotation maneuver from low altitude (Ref. 1).

Perhaps the most important factor in ensuring a successful autorotation outcome is a fast pilot reaction time in taking the appropriate control action. However, in DVE, pilot workload can be extremely high and reaction times may suffer as a result. In non-emergency operations in DVE, stability augmentation systems have reduced pilot workload and contributed to improved safety. The same cannot be said of autorotation scenarios, where no similar augmentation system exists. The purpose of this paper is to report upon an early assessment of a new visual pilot cueing technology that seeks to reduce pilot workload and improve the prospects for a successful autorotation landing.

The idea of autorotation control is not new and has been the subject of extensive research. Lee *et al* (Ref. 2) investigated the problem of autorotation using an optimal control approach, and showed that the height-velocity avoid region could be significantly reduced using automatic control. Abbeel *et al* (Ref. 3) created a reinforcement learning controller that uses data derived from human-piloted autorotation trajectories. Dalamagkis *et al* (Ref. 4) investigated the use of artificial neural networks for the problem of one-dimensional autorotation along the vertical axis only. More recently, Yomchinda *et al* (Ref. 5) and

Presented at the AHS International 73rd Annual Forum & Technology Display, Fort Worth, Texas, USA, May 9-11, 2017.

Tierney and Langelaan (Ref. 6) considered the problem of trajectory path planning during autorotation, using a reachable set formulation to calculate the set of flare entry points from which a helicopter can safely land.

While these authors have considered the problem of autonomous autorotation, additional work has investigated the possibility for pilot cueing and improved situational awareness. Keller *et al* (Ref. 7) examined active inceptor concepts for autorotation pilot cueing, using simple heuristic criteria to determine if the aircraft is approaching a dangerous state. Bachelder *et al* (Ref. 8) developed a pilot cueing system which uses an iterative optimization scheme to derive autorotation trajectories. Recently, the Helicopter Active Control Technology Program (HACT) at Boeing (Ref. 9) addressed the problem of tactile feedback during autorotation using a specially-trained neural network, although this system addressed steady-state descent only.

While a significant body of work exists on the topic of autorotation control, several factors have limited the practical utility of previous approaches. One factor is that the use of iterative optimization algorithms may limit the ability to derive convergence guarantees needed for certification and operational use. Another issue is that any production pilot cueing system must provide valid pilot guidance throughout the flight envelope, even in low-energy flight conditions where a fully-survivable autorotation may not be possible. Deriving control laws to provide valid pilot guidance from any general flight scenario has proven to be a difficult task. One control law that has been at least partially successful in achieving this generality is the recent multi-phase controller developed by Sunberg *et al* (Ref. 10, 11). This control law uses a multi-phase tiered logic approach to generate control inputs during autorotation and exhibits deterministic runtime and guaranteed convergence. A unique feature of this algorithm is its use of time-to-ground-contact estimates to shape the final flare trajectory. These control calculations based on time-to-contact are similar in nature to the tau-based flight guidance strategies developed by Jump and Padfield (Ref. 12-14) for aircraft flare maneuvers. The use of time-to-contact in the flare control formulation in Refs. 10 and 11 allows the resulting control law to generate suitable flare trajectories from almost any point in the vehicle state space, providing the needed generality for use in operational pilot cueing systems.

The control algorithm of Refs. 10 – 11 was formulated for use in autonomous helicopter autorotation maneuvers. This paper describes the results of a first attempt to use the control algorithm for pilot-in-the-loop flight. The algorithm has been used to drive a visual display-based autorotation cueing system. The cueing system presents the pilot with the desired longitudinal cyclic and collective inputs for a safe helicopter autorotation and landing. It has been implemented within the University of Liverpool's HELIFLIGHT-R simulation environment (Ref. 15). A series of simulator flight experiments performed in the HELIFLIGHT-R simulator are documented, in which engineer pilots attempt to enter and successfully complete an autorotation manuever using a Flightlab Generic Rotorcraft (FGR) model (which is based on the UH-60), with and without the pilot cueing system in Good and Degraded Visual Environments.

The usual start point for a handling qualities evaluation would be Ref. 16. However, Ref. 16 does not have a specific Autorotation Maneuver Mission Task Element (MTE). Therefore, performance of pilot-in-the-loop autorotation maneuvers with and without the pilot cueing system was evaluated based on both subjective pilot feedback and objective measurements of landing survivability metrics defined in Ref. 11 and listed in Table 1. These relate to the helicopter's final state at ground contact against acceptable ranges for aircraft and crew survivability. Using these as a basis, the efficacy of the cueing environment has been evaluated by comparing the results achieved between test cases performed with and without the cueing system. Areas for continuing research are then discussed.

Table 1. Conditions for Successful and Marginal Landings

Parameter	Condition for successful landing	Condition for Marginal Landing
Pitch Angle θ	$<12^o$	$<20^o$
Forward Speed V_{des}	<30 knots	< 60 knots
Vertical Speed Zdot	< 8 ft/s	<15 ft/s
Pitch Rate q	$-30^o/s < q < 20^o/s$	$-50^o/s < q < 40^o/s$

CONTROL LAW FORMULATION

The autorotation control law formulation is based on that described in Refs. 10 and 11, and is summarized here. The control law is designed to interface with a standard autopilot or stability and control augmentation system (SCAS) capable of accepting translational rate commands (TRC). Figure 1 shows how the autorotation control law interfaces with a TRC system. At each control update during autorotation, the autorotation controller provides three outputs. The first is the derivative of the collective control ($\dot{\theta}_0$), which can be integrated to form the collective stick command. The second output is a forward speed command, labeled V_{des}, which is tracked by the autopilot or TRC SCAS. The final output, labeled η_{max}, is the maximum allowable aircraft pitch angle. This is used to adjust the saturation limit in the TRC system. As an example, if the autorotation controller is commanding a V_{des} much less than the current speed (so that a decelerating pitch up is required), the autopilot controller is restricted to pitch angles no greater than η_{max}. This is included in the controller to avoid large pitch angles as the vehicle nears contact with the ground. Note that, for the automatic flight case, the autopilot controller is assumed to be already available and is not described here. An example description of such a control algorithm is available in Ref. 10. Also note that the lateral

cyclic and pedal channels are not considered in this analysis, and are free for manipulation to (for instance) bank the aircraft toward a selected landing site.

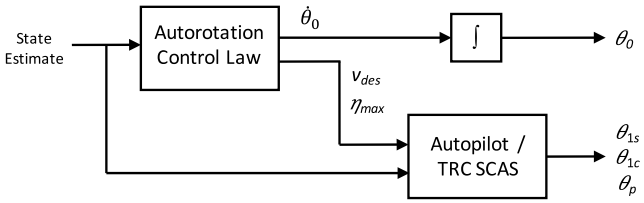

Figure 1 Autorotation Controller Integration with Autopilot.

The autorotation control law is formulated as a multi-phase algorithm, which each phase corresponds to a specific portion of the maneuver. There is a specific control law for determining $\dot{\theta}_0$, V_{des}, and η_{max} which is valid in each phase. Three main phases are defined as: steady-state, flare, and touchdown. Two additional phases, pre-flare and landing, are used to facilitate transitions between the three main phases. The controller progresses between each phase based on altitude and predicted time-to-ground contact criteria. A set of altitude criteria are defined which dictates the altitudes over which each phase is active. Likewise, a set of time-to-contact criteria are defined over which each phase is active. If either the altitude or the time-to-contact criteria are satisfied for a phase transition to occur, the controller transitions to the next phase. Backward phase transitions are not allowed. When phase transitions occur, they do so in a fuzzy manner so that each phase has partial authority during the transition. Figure 2 shows a schematic of the phases and the general regions of the state space over which they are defined.

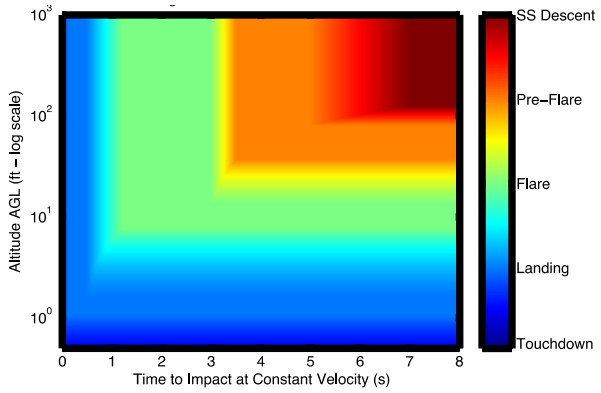

Figure 2. Phase Transition Diagram for Autorotation Control Law.

The specific values on this plot are those used in Ref. 10 for the AH-1G Cobra aircraft, and differ from the values for the UH-60 used here. More information regarding this fuzzy blending scheme is available in Ref. 10. Note that these phase transition values are tuning parameters that must be defined for a specific aircraft.

As an example of one of the phase control laws, consider the controller associated with the steady state phase. In this phase, the following control laws are applied:

$$\dot{\theta}_0 = \hat{k}_d \dot{\Omega} + \hat{k}_p \left(\Omega - \hat{\Omega}_{des} \right) \tag{1}$$

$$v_{des} = \hat{v}_{ss} \tag{2}$$

where values with a (^) denote a controller tuning parameter and Ω is the main rotor rotation rate. Here $\hat{\Omega}_{des}$ and $\hat{v}_{ss}$ are the desired rotor speed and the desired forward flight speed during steady state autorotation descent, respectively. During the steady state phase, no limit is placed on η_{max} and thus the autopilot or TRC SCAS uses its default saturation value for pitch angle commands.

The flare phase controller differs quite substantially from the steady state phase. This is due to the fact that the flare trajectory must be adjusted according to the total kinetic energy with which the vehicle approaches the ground. Proper adjustment of the flare trajectory ensures that the controller is robust to various initial flight conditions at the onset of autorotation. During the flare phase, the controller adjusts the collective so as to track a desired time-to-ground contact. This desired time is given by,

$$t_{gc} = \hat{t}_{le,\max} \times \min\left(1, \max\left(0, \alpha\right)\right) + \hat{t}_l \tag{3}$$

where $\hat{t}_{le,\max}$ and $\hat{t}_l$ are tuning parameters which bound the length of the overall flare, and $\alpha \in [0,1]$ is a value computed based on the total helicopter kinetic energy (which includes translational and rotor rotational kinetic energies). The formula for computing α is omitted here but is given in Ref. 10. Once t_{gc} is determined, a desired vertical acceleration is computed according to,

$$\ddot{h}_{des} = -\frac{2}{t_{gc}^2} h - \frac{2}{t_{gc}} \dot{h} \tag{5}$$

where h is the current helicopter altitude. This provides the constant vertical acceleration needed to achieve ground contact at a time t_{gc} in the future. The collective control law is then defined which drives the actual vertical acceleration to the desired acceleration, given by,

$$\dot{\theta}_0 = \hat{k}_{p\theta} \left(\ddot{h}_{des} - \ddot{h} \right) \tag{6}$$

Finally,

$$v_{des} = \hat{v}_{td} \tag{7}$$

where $\hat{v}_{td}$ is the desired forward speed at touchdown. As in the steady-state phase, no limit is placed on η_{max}.

The touchdown phase is fully active only when the helicopter is very near the ground, usually within 10-20 ft.

This phase uses the same forward speed command as in Equation (7). In the touchdown, an open-loop collective control is defined as,

$$\dot{\theta}_0 = \hat{\dot{\theta}}_{0,td} \tag{8}$$

where $\hat{\dot{\theta}}_{0,td}$ is a small negative constant (resulting in a slow continual collective decrease). The maximum pitch angle η_{max} is given by,

$$\eta_{\max} = \hat{\eta}_{\max,td} \tag{8}$$

Where $\hat{\eta}_{\max,td}$ is usually only a few degrees, causing the vehicle to land at a nearly level pitch attitude even if excess forward speed is present. A complete description of these phase control laws, as well as the pre-flare and landing phase controllers, are provided in Reference 10.

As shown in Reference 10, this autorotation control law can be generalized to a wide array of flight platforms by appropriate adjustment of the controller tuning parameters. In previous work (Refs. 10 and 11) the authors demonstrated in simulation that the controller can successfully land various classes of vehicles (exemplified by the AH-1G Cobra, and a small RC-sized autonomous helicopter) from a wide range of autorotation entry flight conditions. These included Monte Carlo simulations which showed that the controller can successfully land the AH-1G from well inside the height-velocity avoid region. A key enabling factor in the robustness of the above algorithm is that the flare trajectory is continually adjusted based on estimates of the time-to-ground contact. This is a unique and defining characteristic of this algorithm compared to prior autorotation control laws. As further validation, Reference 10 describes experimental studies in which the controller was repeatedly used to successfully land an RC helicopter in autorotation flight experiments. As will be shown in the subsequent simulation results, the above controller generalizes to larger aircraft such as the UH-60 with appropriate tuning of the controller parameters.

In the current work, the above controller is used both in simulated autonomous landing experiments and to drive a cockpit display in pilot-in-the-loop simulations as described later. When used in conjunction with the cockpit display, the control algorithm is queried at a rate of 20 Hz, providing a collective and cyclic output for display as the requested control input position. A significant benefit of the above control law is that a single control cycle takes very little computational effort and has deterministic runtime – thus high update rates are easily achievable.

SIMULATION MODEL

The control algorithm has been incorporated into the FLIGHTLAB simulation environment using the Control System Graphical Editor (CSGE) (part of the FLIGHTLAB software suite) and attached to the FGR model which is based on the UH-60. Verification of the implementation was made by trimming the model on an 18° glideslope and recording outputs from the control system as the controller processed through the flight phases, and replaying these through the Matlab® version of the controller provided to the University of Liverpool by the Georgia Institute of Technology. Figure 3 demonstrates the correctness of the implementation in FLIGHTLAB, whereby the identical collective and longitudinal cyclic pitch control outputs/demands are generated in both the FLIGHTLAB and Matlab® models. The fact that both traces overlay in Figure 3 demonstrates that both the FLIGHTLAB and Matlab® implementations of the controller provide identical outputs, indicating that the CSGE implementation is correct.

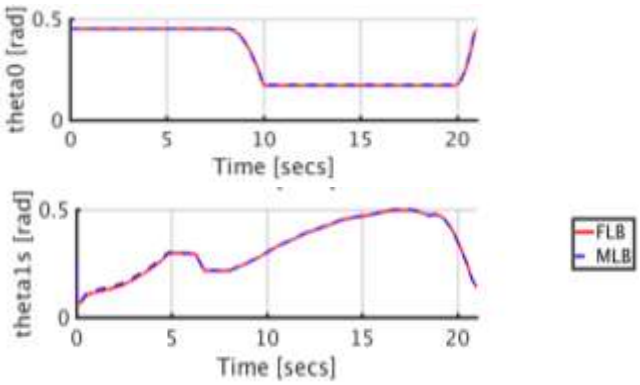

Figure 3. Verification of Controller Implementation within the Flightlab CSGE tool (FLB = FLIGHTLAB Software, MLB = Matlab controller implementation).

The controller implementation allows analysis of both automatic and pilot-in-the-loop autorotation maneuvers. For an automatic landing, the 'desired' longitudinal cyclic and collective blade angles are calculated at each time step by the automated control system and are fed back as inputs to the actuators. For pilot-in-the-loop simulations, this link is deselected and the desired control surface positions are displayed on the HUD in conjunction with the corresponding current control surface positions.

To assist with the tuning process and to demonstrate that the controller is able to guide the aircraft model to a safe landing, the controller was first tuned for an automatic autorotation. A phase-by-phase process was adopted for tuning the model, whereby the controller was first tuned for the steady state and pre-flare flight phases followed by the flare, landing and touchdown phases. These tuning settings were subsequently used for the pilot-in-the-loop simulations. A summary of the tuned control parameters is provided in Table 2. In addition, for all results presented, all lateral aircraft states were locked to allow a focused analysis of the engineer pilot's ability to utilize the information displayed by the controller in the longitudinal axis only. Results from the tuning process yielded the simulation time-histories illustrated in Figure 4 and the performance metrics recorded in Table 3. A brief analysis shows that a descent rate of approximately 39ft/s, forward groundspeed of 105ft/s and

constant rotor speed just under the desired controller set-point of 26rads/s were maintained in the steady state descent. A maximum pitch angle of 21° was reached in the flare stage by applying only a few degrees of longitudinal cyclic. Finally the controller rapidly increased collective demand by approximately two thirds of the available range to arrest the descent rate whilst pushing the stick forward (negative longitudinal cyclic) to bring the aircraft level for landing. One anomaly that can be seen in both the desired collective pitch and longitudinal cyclic which are fed back into the system as control inputs, are the well damped high frequency oscillation when the engine failure occurs and for longitudinal cyclic only when the flare phase is initiated. It is expected that this can be eliminated in future work with further tuning of the control parameters. The performance metrics have been calculated by determining the time at which the aircraft first makes contact with the ground. The data recorded at the previous time-step is then used to determine if the landing was successful, marginal or unsuccessful in comparison with the survivability performance criteria listed in Table 1. The performance metrics are recorded in Table 3 demonstrating that all successful landing criteria have been achieved.

Table 2. Autorotation Controller Parameters

Parameter	Definition	Value
RPM_Auto	Desired main rotor rotation rate for the steady state phase	26 rad/s
K_D_SS	rotor speed time derivative Gain for steady-state descent collective control	$0.1s^{-1}$
K_P_SS	Gain on rotor speed for collective control during steady-state descent	0.015 [nd]
TTI_L	Desired time to impact during the landing phase	2 s
TTI_F_MAX	Maximum cap on the desired time to impact during the flare phase	7 s
K_COL	Rotor collective gain for flare and landing phases	$3.7x10^{-4}$ rad·s^2/ft
TAU	Rotor collective adjustment time constant for flare and landing	0.8 s
FAST_COL_INCREASE	Collective adjustment rate for rapid adjustments during the flare and landing	20°/s
$U_{touchdown}$	Desired forward velocity at touchdown	20 ft/s
U_{auto}	Desired forward speed for the steady state phase	105 ft/s
Landing Max Angle	Maximum cap on pitch angle during the landing phase	12°
Touchdown Max Angle	Maximum cap on pitch angle during the touchdown phase	1°
Touchdown Col Increase	Constant collective pitch rate during touchdown phase	1°/s

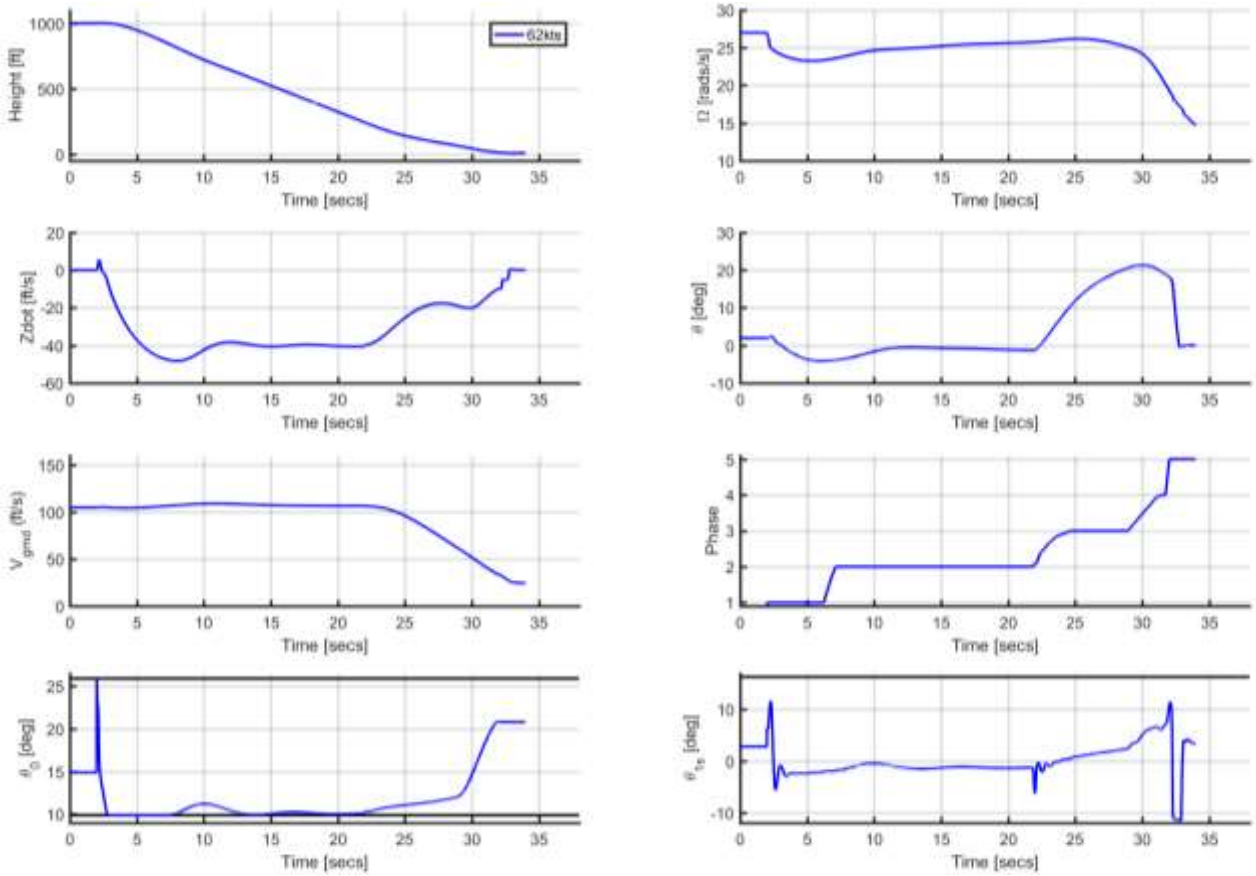

Figure 4. Automatic Autorotation with the FGR Model with Design Point Start Conditions

Robustness Tests

Although the aim of this study is to determine how well the pilot can follow the desired control strategy from the design point, in this case 62knots, automatic controller performance was tested for a range of initial conditions to verify that the controller would, in principle, be capable of guiding the pilot to a successful autorotation maneuver conclusion if the vehicle states were off the design points. Figure 5 illustrates the time-histories recorded when the initial condition was set as 40, 60 and 80 knots, starting at the same altitude of 1000 feet. The controller works to gain the target rotor speed, ground speed and vertical speed in order to store the energy needed for the flare in the rotor. For example, the 40knot case shows an exchange of potential for kinetic energy as the aircraft descent rate is rapidly increased to gain the desired ground speed before settling to the desired descent rate. From this point on, all cases exhibit the same characteristics as the aircraft automatically passes through the later phases of the autorotation maneuver. The primary difference between the cases occurs during the touchdown phase where, depending on the state the aircraft is in when the flare is initiated, the controller response yields the survivable values listed in Table 3. Large variations between the cases are recorded for pitch angle on touchdown. This is due to the controller working with a constant z-axis gear offset from the center of gravity (cg). However, as the aircraft has a pitch nose up attitude at the end of the flare, the z-axis gear offset from the cg increases. This has resulted in the tail landing gear contacting the ground before the controller has had time to reduce the landing pitch attitude for the 40 knot initial condition case.

Table 3. Touchdown Performance Metrics for automatic Autorotation

Initial Velocity [knots]	Ground Speed [knots]	Descent Rate [ft/s]	Pitch Angle [deg]	Pitch Rate [deg/s]
62	16	0.35	-0.2	-0.1
40	26	0.6	-10	12
60	16	0.4	0	-0.3
80	18	9	15	-3.2

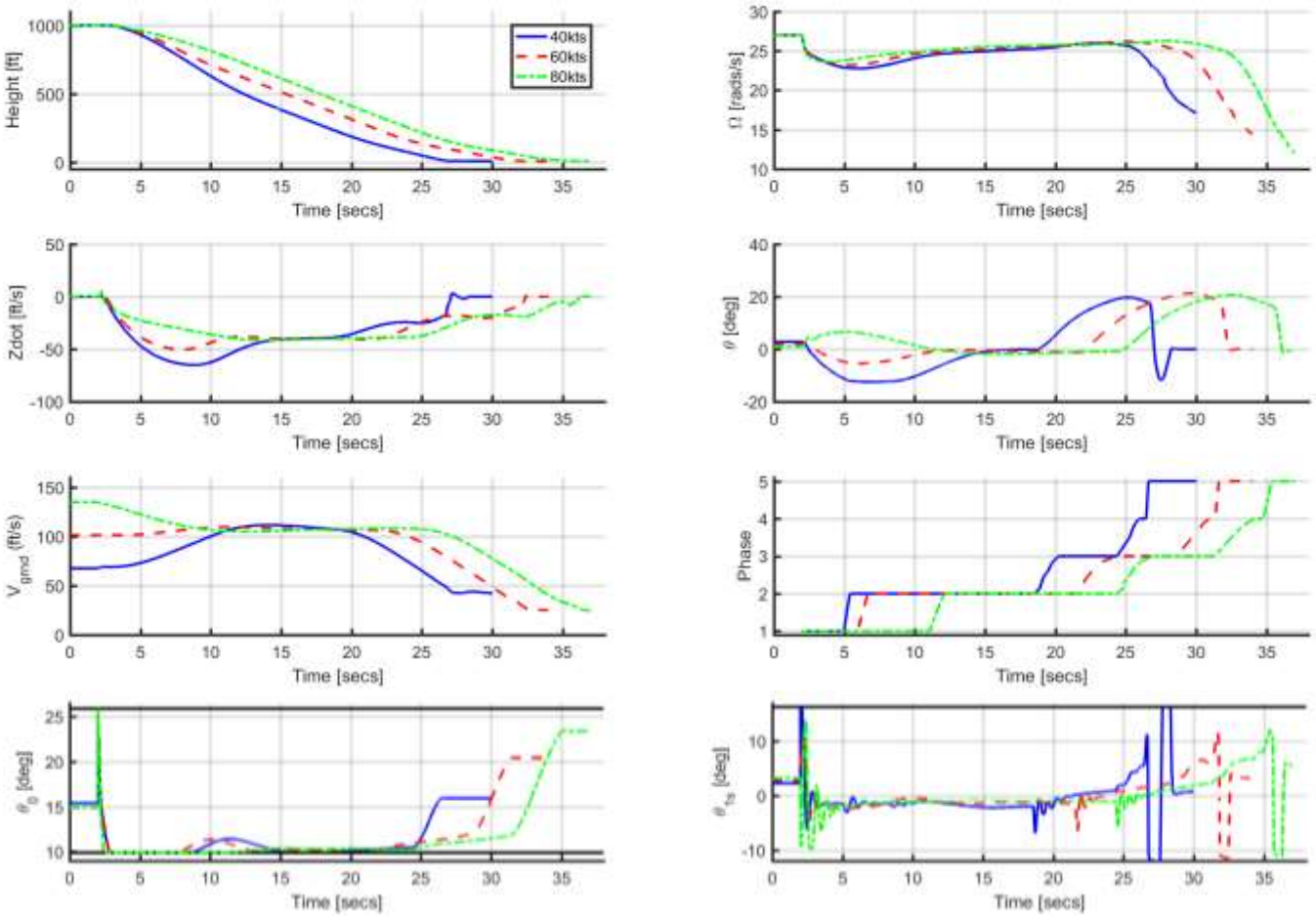

Figure 5. Automatic Autorotation with the FGR Model with Off-Design Point Start Conditions

PILOT-IN-THE-LOOP SIMULATION

For the purposes of performing human-in-the-loop testing, a simple visual display system was implemented in the University of Liverpool's HELIFLIGHT-R full-motion simulator, Figure 6. HELIFLIGHT-R features a three channel 220 x 70 degree field of view visual system, a four-axis force feedback control loading system and an interchangeable crew station. The outside world imagery is generated using Presagis' Creator Pro software to produce either geo-specific or custom visual databases. Using Presagis' VEGA Prime software, the Liverpool Flight Science & Technology Group has generated its own run-time environment[16], LIVE (Liverpool Virtual Environment) which allows the simulator operator to change environmental effects such as daylight, cloud, rain and fog. A Heads-Up Display (HUD) can either be generated using an LCD screen with a beam splitter located above the instrument panel or projected directly onto the dome. The latter case was used for the results reported in this paper. The motion and visual cues, together with appropriate audio cues, provide an immersive environment for a pilot. Data from the flight models, e.g. aircraft accelerations, attitudes etc., together with pilot control inputs, can be monitored in real-time and recorded for post-flight data analysis.

Figure 7 shows a screen-shot of the HUD created using VAPS XT. It consists of the usual basic pilotage information (speed, altitude, heading, horizon bar etc.). However, it also contains four additional symbols that provide autorotation cueing information to the pilot. These are highlighted in Figure 7. Two symbols provide visual information as to the current actual longitudinal cyclic and collective positions whilst the other two symbols provide the desired cyclic and collective control positions, derived from the autorotation algorithm output. The pilot's task is to overlay the desired and actual position for each control inceptor for each phase of the maneuver, from the beginning of autorotation through to touchdown. Autorotation's were attempted by three engineer pilots who all have some real world private pilot level fixed- or rotary-wing flying experience, with and without the pilot cueing system in GVE = 1 and DVE = 3, as defined in Ref. 17.

Autorotation with No Visual Aid in GVE

Following a brief on the principle of flying an autorotation maneuver, a minimum of five autorotation's were flown by each pilot in a GVE. An example of the performance by each pilot is shown in Figure 8. Touchdown metrics are recorded in Table 4. It can be seen that when the engine failure is applied, the pilots lower collective to/close to the minimum and regulate speed with longitudinal cyclic as expected. Following an initial transient and an oscillatory response on the longitudinal cyclic, the pilots are able to settle into a steady state descent at approximately the required rotor speed and at a forward speed of around 63 knots. This resulted in a descent rate of around 2400 feet per minute. The flare should be initiated approximately 150ft above ground level. However, it can be determined from Figure 8 that all pilots initiated the flare at a much lower altitude, resulting in their landings being classified as marginal, as per the values of Table 1.

Autorotation with the Visual Aid in GVE

With the visual cueing system switched on, pilots again flew a minimum of 5 test points. Again, a typical example of the recorded time histories is plotted in Figure 9 and Figure 10. Figure 9 illustrates the aircraft states while Figure 10 provides a comparison of control surface position as commanded by the pilot (solid line) and the desired position calculated by the algorithm and displayed on the HUD. The pilots still maintain ground and descent speed in the steady state and pre-flare phases, but this time they also use collective to maintain tighter control over the desired rotor speed. Both engineer pilot and flight control system achieve the steady state descent in approximately the same timeframe and with a very similar result (approx. 62 knots and 2400 ft/min). Pilots commented that in these phases it was not easy an easy task to obtain and hold the desired longitudinal control surface position. Consequently, the strategy adopted was to apply only small correctional inputs and let the desired position symbol converge on the actual position symbol. This is particularly evident in the longitudinal cyclic plots in Figure 10. When entering the flare, the desired collective position indicator moved very rapidly to its limits and could not be tracked by the pilot. Nevertheless, this rapid symbol movement did prove to be a useful indication as to when to initiate the flare. The result is a more gentle flare than for the case with no visual aid, culminating in more consistent and successful landings.

It was noted by the engineer pilots that tracking the two different symbols simultaneously was quite difficult and did not lend itself to looking at the outside world, to scan for available landing sites, for example. Modification to the cueing symbol dynamics was recommended to assist with the reduction in the pilot's workload in this regard.

Autorotation with Visual Aid in DVE

To assess the 'stretch' potential of the system, it was also tested in Level 3 DVE by introducing a low cloud level and fog to obscure the horizon and runway landing site. Three engineer pilots flew the autorotation maneuver to a landing a minimum of five times. Example typical time- histories are plotted as Figure 11 and Figure 12, whilst touchdown performance is again shown in Table 4. Analysis of the time histories shows that the pilots employed the same strategy used in GVE. However, it is evident from the touchdown performance metrics that the pilots generally performed as well in DVE as in GVE. Pilots commented that this was due to elements of workload actually decreasing as they were compelled to use only the visual cueing system as other external visual cues were no longer available to distract them. They also commented that they were helped by flying the GVE sessions first and so had 'learned' what sort of control inputs to make (magnitude and rate) at flare initiation.

One issue that is evident in the piloted results in Figures 10 and 12 is that the longitudinal cyclic command requested by the control algorithm is extremely high at the initiation of the flare (saturating the control input). This is because the velocity tracking gains of the autorotation controller are tuned for automated landing performance, and are thus rather aggressive. During the autonomous control results in Figures 4 and 5, the longitudinal cyclic does not reach its saturation limit, although as observed before, a heavily damped perturbation is noted. On the other hand, with the human pilot in the loop, it is clear that these same velocity tracking gains are no longer appropriate. New gains will need to be selected to avoid recommending that the pilot provide full aft cyclic stick. Future work will explore alternative methodologies for selecting (less aggressive) gains for the velocity tracking loop but that cue the pilot effectively during execution of the flare maneuver.

Figure 6. HELIFLIGHT-R simulator – internal and external views

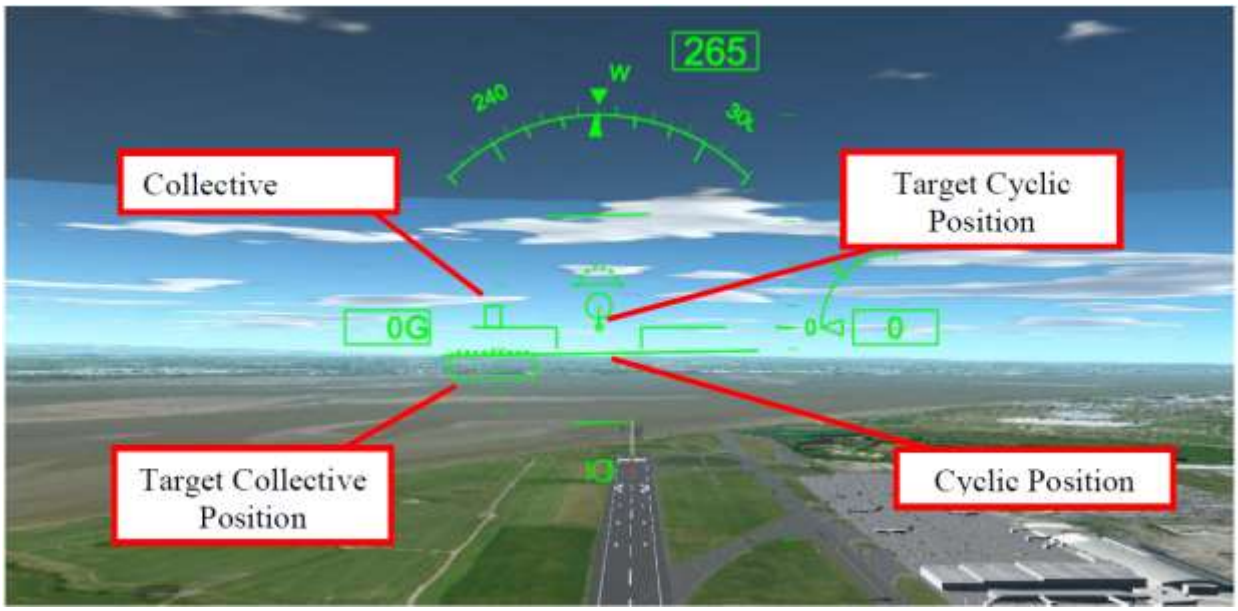

Figure 7. Preliminary display to provide helicopter autorotation inceptor cueing to the pilot

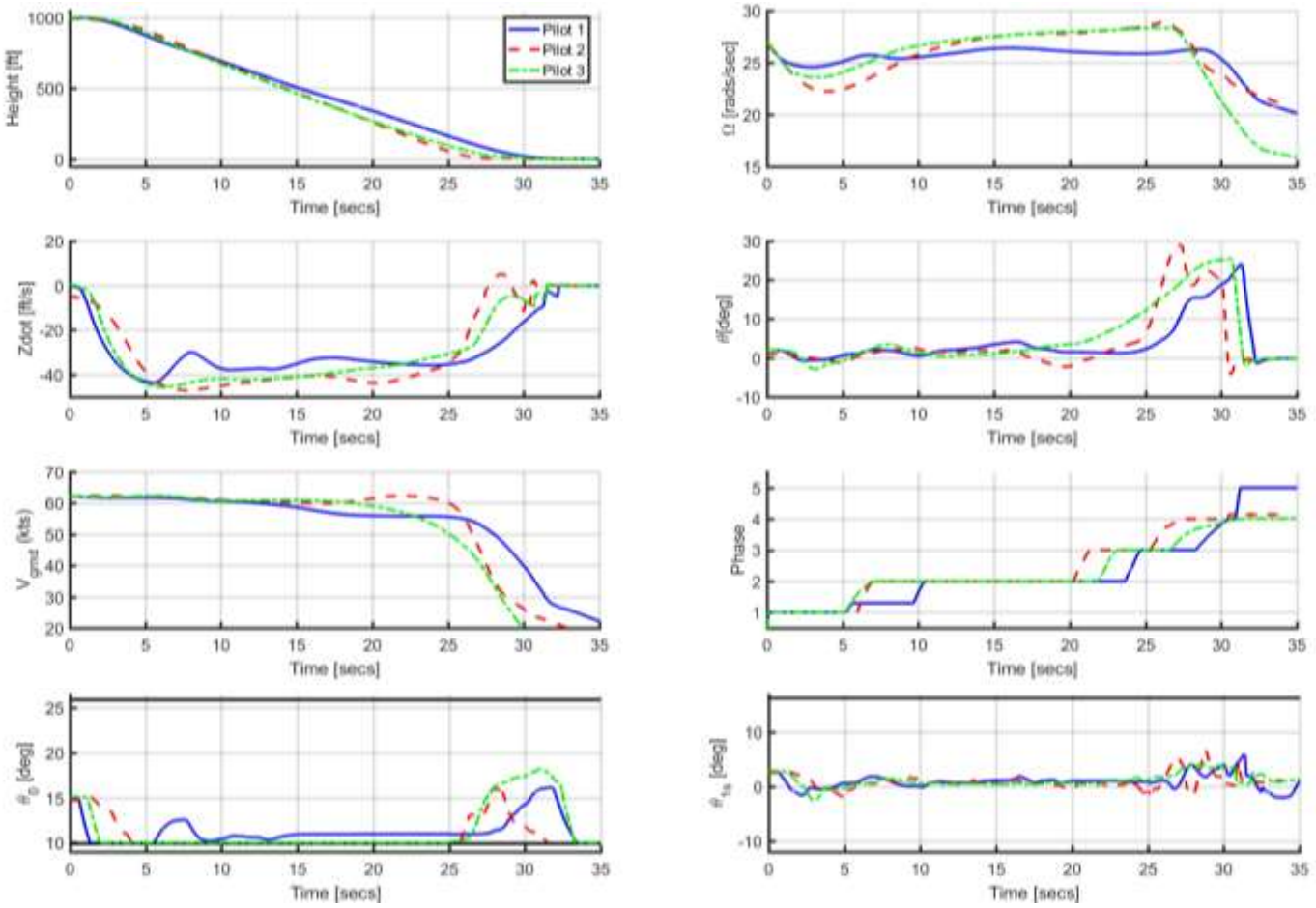

Figure 8. Pilot-in-the-Loop Autorotation with no Aid

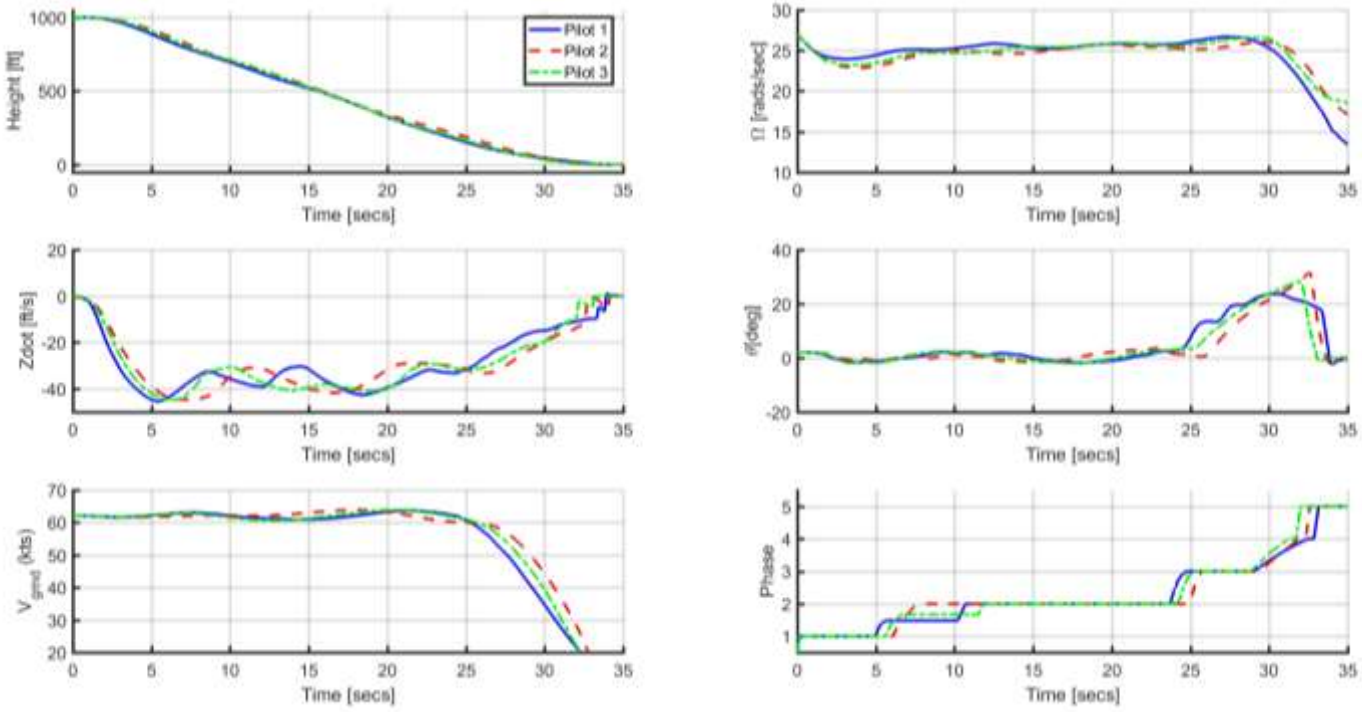

Figure 9. Pilot-in-the-Loop autorotation with visual Aid Engaged

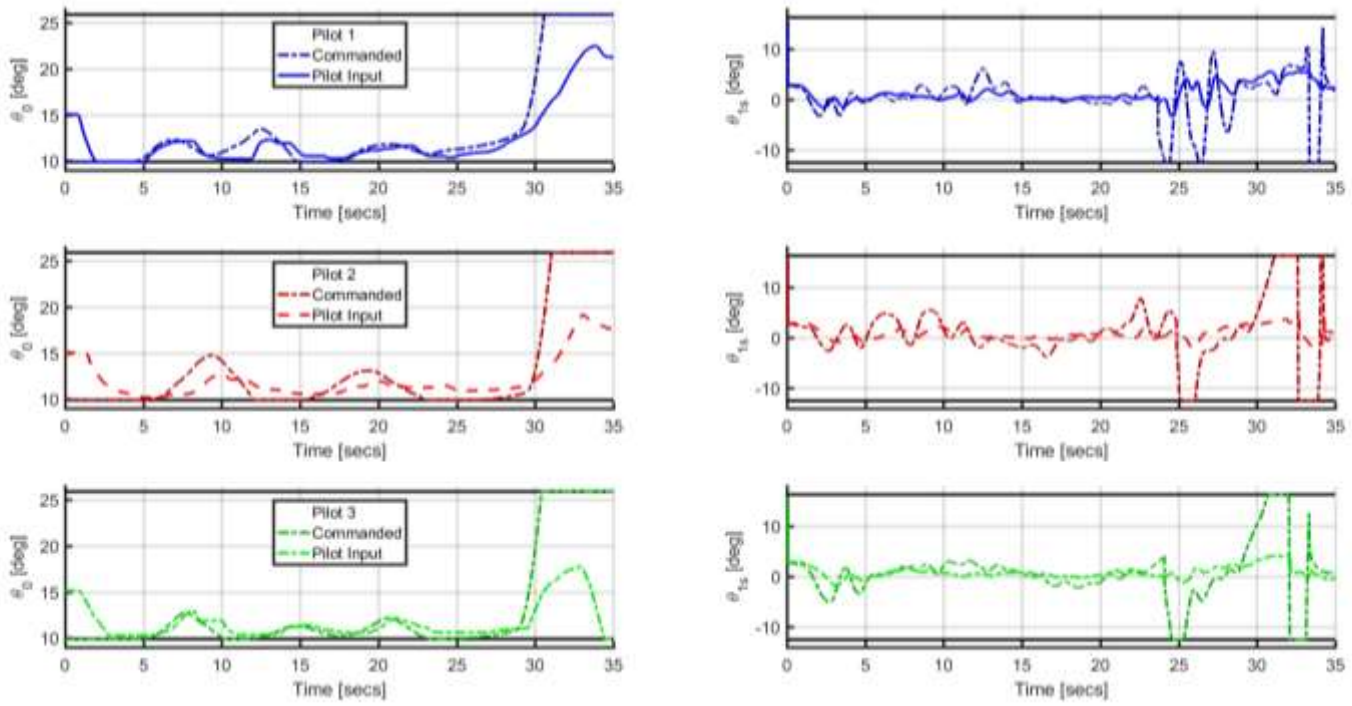

Figure 10. Comparison of actual and desired Pilot control inputs for Pilot-in-the-Loop autorotation with visual Aid Engaged

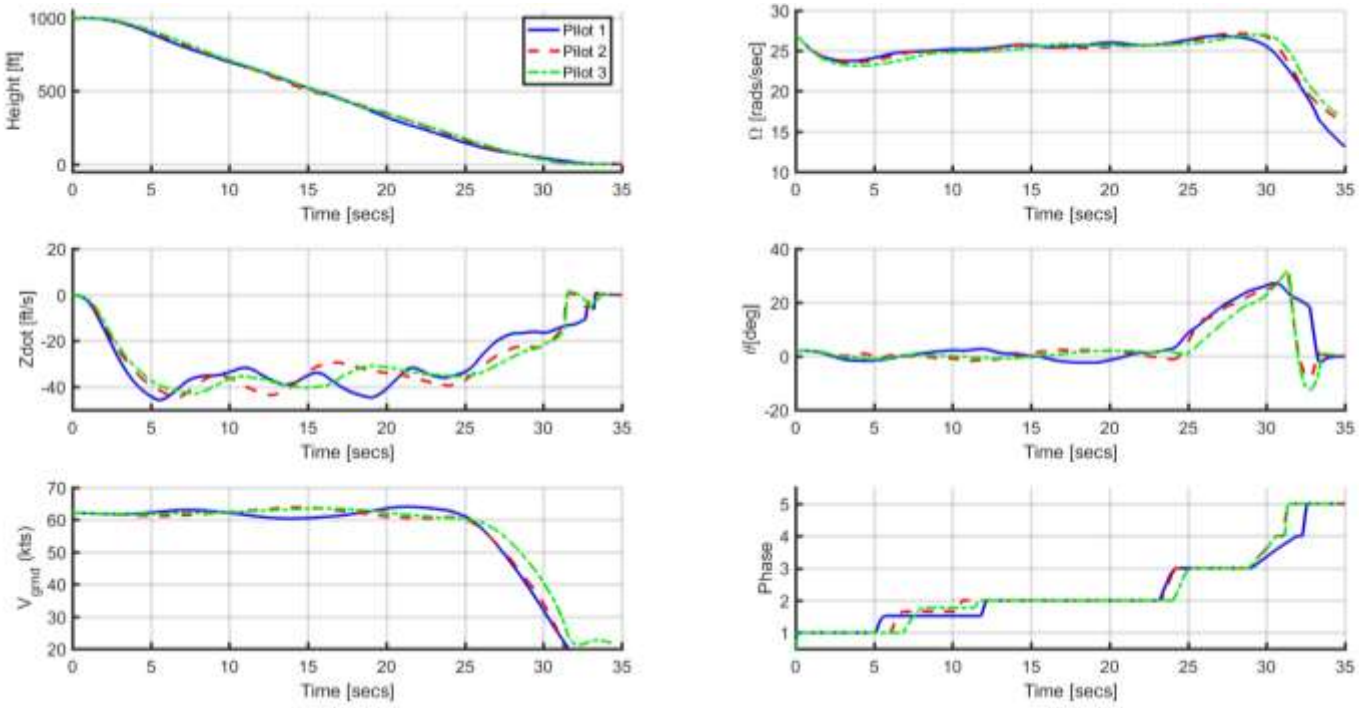

Figure 11. Pilot-in-the-Loop autorotation with visual Aid Engaged in DVE

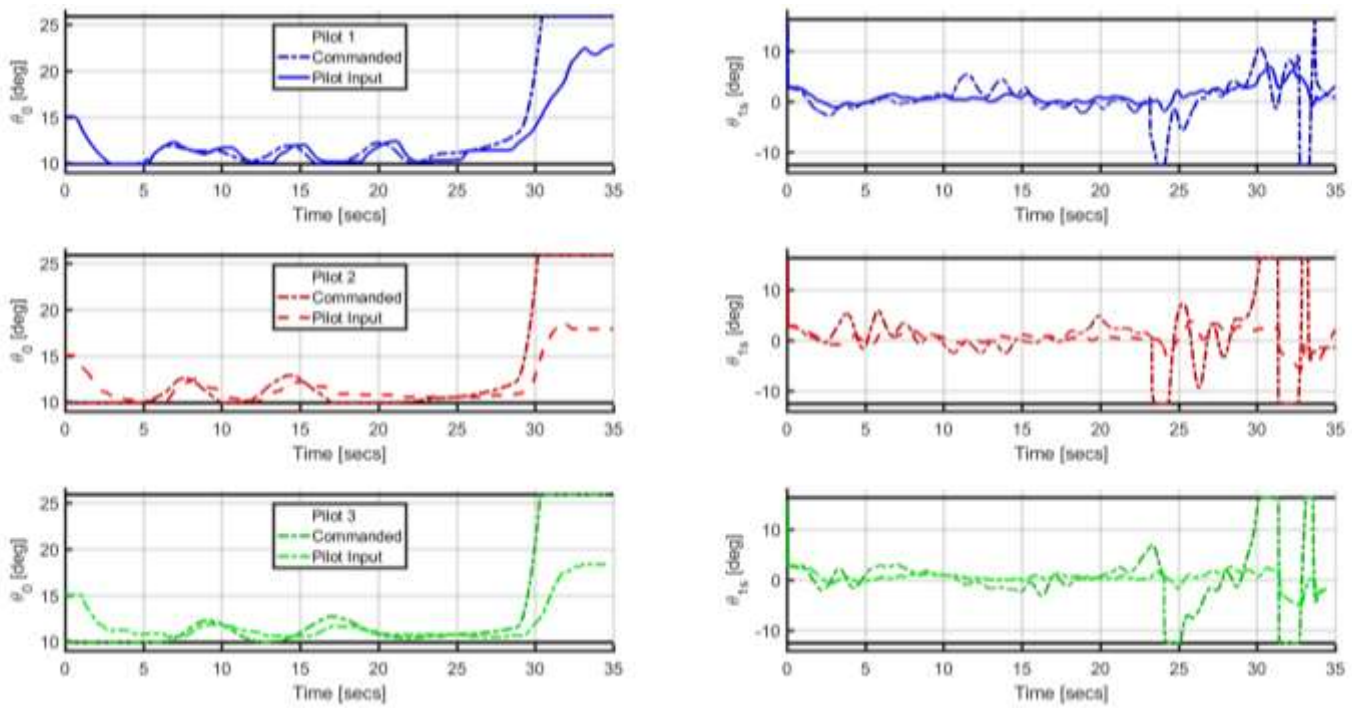

Figure 12. Comparison of actual and desired Pilot control inputs for Pilot-in-the-Loop autorotation with visual Aid Engaged in DVE

Table 4. Touchdown Performance for Pilot-in-the-Loop Autorotation

Test Case	Pilot	Ground Speed [knots]	TD Zdot [ft/s]	Pitch Angle [deg]	Pitch Rate [deg/s]
GVE	1	28	4	8	-24
/ OFF	2	24	1	-3	12
	3	13	5	11	-35
GVE	1	13	1	-2	6
/ ON	2	16	6	-3	-1
	3	17	5	4	18
DVE	1	12	1	-1	8
/ ON	2	15	2	-1	28
	3	22	2	-1	29

CONCLUDING REMARKS

This short study to date has explored the translation of an autonomous autorotation controller to drive a visual cueing system to guide a pilot through the desired control inputs to achieve a successful autorotation.

The work has been broken down into four distinct tasks including configuring the control law to interface with a cockpit display; development of a basic display to provide autorotation cueing to the pilot using the control law as input; integrating the control law into the HELIFLIGHT-R simulation facility and finally performing simulated flight tests to evaluate the performance of the autorotation algorithm in both GVE and DVE.

The results presented were based on the original tuning of the automated system which was then flown by engineer pilots. It was found that the demanded longitudinal cyclic, in particular, was difficult to track. Thus, the pilots adopted a strategy whereby only small correcting inputs were applied to allow the desired control demand symbol to converge on the current control position symbol. However, all engineer pilots utilized the cueing system to initiate the flare in a timelier manner, resulting in a more gentle flare, culminating in more consistent and successful landings in GVE. Touchdown performance in DVE was as good as in GVE as the pilots were obligated to use only the visual cueing system, as other outside world visual cues were obscured.

The next stage of the work is to ensure that all phases of the autorotation maneuver algorithm can be tracked by a human-in-the-loop rather than an automatic flight control system whilst retaining survivable autorotation performance.

Author contact:
Jonathan Rogers jonathan.rogers@me.gatech.edu,
Neil Cameron ncameron@liverpool.ac.uk
Mike Jump mjump1@liverpool.ac.uk

ACKNOWLEDGMENTS

The authors are grateful to John Preston/Amanda Napier and the U.S. Army Missile and Aviation Research Development and Engineering Command (AMRDEC) for their support of this research. Thanks also to the University of Liverpool ‘engineer pilots’ for their support.

REFERENCES

[1]Military Times, "Investigators: Human Error Caused Idaho Guard Helo Crash," February 8, 2015, Accessed Online 12 September 2016.

[2]Lee, A. Y., Bryson, A. E., and Hindson, W. S., "Optimal Landing of a Helicopter in Autorotation," *Journal of Guidance, Control, and Dynamics*, Vol. 11, No. 1, 1988, pp. 7–12.

[3]Abbeel, P., Coates, A., Hunter, T., and Ng, A. Y., "Autonomous Autorotation of an RC Helicopter," *Experimental Robotics*, Vol. 54, 2009, pp. 385–394.

[4]Dalamagkidis, K., Valavanis, K. P., and Piegl, L. A., "Autonomous Autorotation of Unmanned Rotorcraft using Nonlinear Model Predictive Control," *Journal of Intelligent and Robotic Systems*, Vol. 57, (1–4), September 2009, pp. 351–369.

[5]Yomchinda, T., Horn, J. F., and Langelaan, J.W., "Flight Path Planning for Descent-Phase Helicopter Autorotation," AIAA Guidance, Navigation, and Control Conference, Portland, OR, August 8–11, 2011, pp. 1–24.

[6]Tierney, S. and Langelaan, J., "Autorotation path planning using backwards reachable set and optimal control," American Helicopter Society Forum, 2010.

[7]Keller, J. D., McKillip, Jr., R. M., Horn, J. F., and Yomchinda, T., "Active Flight Control and Applique Inceptor Concepts for Autorotation Performance Enhancement," AHS International 67th Annual Forum Proceedings, Virginia Beach, VA, May 3–5, 2011.

[8]Bachelder, E. N., Lee, D.-C., and Aponso, B. L., "Autorotation Flight Control System," U.S. Patent 7976310 B2, 2011.

[9]Nicholas, J., and Miller, D., "Method, system, and computer program product for tactile cueing flight control," U.S. Patent 6735500 B2, 2004.

[10]Sunberg, Z., Miller, N., and Rogers, J., "A Real Time Expert Control System for Helicopter Autorotation," *Journal of the American Helicopter Society*, Vol. 60, 2015, pp. 1-15.

[11]Sunberg, Z., Miller, N., and Rogers, J., "A Real Time Expert Control System for Helicopter Autorotation," 70th Forum of the AHS, Montreal, Canada, May 20-22, 2014.

[12]Jump, M., and Padfield, G. D., "Investigation of the Flare Maneuver Using Optical Tau," *Journal of Guidance, Control, and Dynamics*, published online Sept. 2006; Vol. 29, No. 5, pp. 1189-1200. doi: 10.2514/1.20012

[13]Jump, M., and Padfield, G. D., "Progress in the Development of Guidance Strategies For the Landing Flare Maneuver Using Tau-based Parameters," *Aircraft Engineering and Aerospace Technology*, published online 2006; Vol. 78, No. 1, pp. 4-12. doi:10.1108/17488840610639618

[14]Padfield G.D., Lu, L., and Jump, M., "Tau Guidance in Boundary-Avoidance Tracking - New Perspectives on Pilot-Induced Oscillations," *Journal of Guidance, Control, and Dynamics*, published online Jan. 2012; Vol. 35, No. 1, pp. 80-92. doi:10.2514/1.54065

[15]White, M.D., Perfect, P., Padfield, G.D., Gubbels, A.W. & Berryman, A.C., Acceptance testing and commissioning of a flight simulator for rotorcraft simulation fidelity research, Proceedings of the IMechE, Part G: Journal of Aerospace Engineering, 2012, **226**, (4), pp 638-686. DOI: https://doi.org/10.1177/0954410012439816

[16]Anon., ADS-33E-PRF, Aeronautical Design Standard, Performance Specification, Handling Qualities Requirements for Military Rotorcraft, United States Army Aviation and Missile Command, Aviation Engineering Directorate, Redstone Arsenal, Alabama, 21 March 2000.

[17]Perfect P, Jump M and White MD, "Methods to Assess the Handling Qualities Requirements for Personal Aerial Vehicles", *AIAA Journal of Guidance and Control, Journal of Guidance, Control, and Dynamics*, Vol. 38, Issue 11 pp. 2161-2172. April 2015, DOI: 10.2514/1.G000862